Int J Adv Manuf Technol (2015) 77:1655–1669
DOI 10.1007/s00170-014-6484-1

ORIGINAL ARTICLE

Experimental investigation of surface integrity in finish dry hard turning of hardened tool steel at different hardness levels

Linhu Tang · Chengxiu Gao · Jianlong Huang · Hao Shen · Xiaojun Lin

Received: 21 June 2014 / Accepted: 7 October 2014 / Published online: 16 November 2014

Abstract In this paper, the influences of cutting speed, depth of cut, feed, workpiece hardness (51, 55, 58, 62, and 65±1 HRC), and nose radius on surface integrity in finish dry hard turning (FDHT) of the hardened tool steel AISI D2 by utilizing the polycrystalline cubic boron nitride (PCBN) inserts were experimentally investigated. Experimental results showed that the ploughing effect, serious squeeze, and elastic deformation have more significant on the surface roughness than those black fusion welding materials and side flows, and the surface roughness values are in the range of 0.34–0.86 μm between 150- and 301-m/min cutting speeds and totally attains a surface finish of grinding. The surface roughness is not very sensitive to the depth of cut in the range from 0.10 to 0.25 mm. The "residual cutting" materials, material plastic deformation, and even cohesion in the machined surface and cold welding effect do occur and hence influence on the surface integrity. The tiny grooves, severe plastic flow, and extensive material flows at lower feeds have significant influence on the surface integrity. The subsurface damages produced by the turning process also do occur and become severer at the larger feeds due to the localized stretch, plastic deformation, and even dilacerations of subsurface material induced by the friction from the tool flank face. The thermal softening, serious material side flows, and squeezing have significant effect on surface integrity when FDHT of the hardened tool steel AISI D2 at different hardness levels. And the heat effect is greater than the geometry effect as the nose radius attains a certain value.

Keywords FDHT · Hardened tool steel · Workpiece hardness · Surface roughness · Surface morphology

Nomenclature

v	Cutting speed (meter per minute)
a_p	Depth of cut (millimeter)
f	Feed (millimeter per revolution)
H	Workpiece hardness (HRC)
r_ε	Nose radius (millimeter)
b	Chamfer width (millimeter)
β	Chamfer angle (degrees)
R_a	Surface roughness (micrometer)
κ_r	Major cutting-edge angle (degrees)
κ_r'	End-cutting edge angle (degrees)
α	Rake angle (degrees)
γ_0	Clearance angle (degrees)
γ_0'	Side clearance angle (degrees)
λ_s	Inclination angle (degrees)

1 Introduction

According to literature [1, 2], the finish dry hard turning (FDHT) is defined as the single-point turning process of materials harder than 50 HRC under the condition of small feed and fine depth of cut by utilizing appropriate cutting tools without or minimizing the use of cutting fluid in order to reach good surface quality, dimensional and form tolerances, and

L. Tang (✉) · C. Gao · X. Lin
Provincial Key Laboratory for Green Cutting Technology and Application of Gansu Province (University), Lanzhou Institute of Technology, Lanzhou, People's Republic of China
e-mail: tanglinhu@126.com

J. Huang · H. Shen
College of Mechano-Electronic, Lanzhou University of Technology, Lanzhou 730050, Gansu Province, People's Republic of China

Present Address:
L. Tang · C. Gao · X. Lin
College of Mechano-Electronic, Lanzhou Institute of Technology, No. 1 Gongjiaping East Road, 730050 Lanzhou, Gansu Province, People's Republic of China

surface integrity close to those obtained grinding. It has gained more attention owing to its substantial advantages, such as reducing the time of finish machining, declining the cost of manufacturing, and eliminating the hazard of cutting fluid by using dry machining compared to grinding [3–5]. Therefore, FDHT has become an alternative machining process for grinding processes of hardened steels due to improvements in the performance of hard-tool materials [6, 7].

Numerous investigations have been carried out to study the surface integrity in turning operations. Thiele et al. [8] have investigated the effects of tool cutting edge geometry and workpiece hardness (41, 47, and 57 HRC) on the surface roughness in finish hard turning of AISI 52100 steel. The results showed that the cutting edge geometry has significant influence on the surface roughness, and that large edge hones lead to higher surface roughness values than small edge hone. Then, Rech et al. [9] have found that hard turning process has capacities to produce a low surface roughness (Ra<0.20 μm) during a long cutting time and also to induce compressive residual stresses when turning of case-hardened 27MnCr5 at low feed rate and low cutting speed. Besides, the effects of cutting edge geometry, workpiece hardness, feed rate, and cutting speed on surface roughness in finish hard turning of AISI H13 steel were experimentally investigated by Ozel et al. [10]. In this study, the results showed that the effects of workpiece hardness, cutting edge geometry, feed rate, and cutting speed on surface roughness are statistically significant. In addition, Umbrello and Jawahir [11] have predicted the white layer formation during machining of hardened AISI 52100 steel with three different hardness levels of 56, 62, and 66 HRC by utilizing a finite element mode; however, it is unrealistic to expect that the same results can be applied to the case of hard turning of other materials. Okada et al. [12] have investigated cutting performance of CBN tools and PVD-coated carbide tools in end-milling of hardened steel. In this study, the influence of workpiece hardness on surface roughness was summarized. Aouici, et al. [13] have experimentally investigated the influences of cutting speed, feed, depth of cut, and workpiece hardness on the surface roughness in turning hardened steel AISI H11. However, workpiece material has only been hardened to the low hardness with 40, 45, and 50 HRC. Later, Rech and Moisan [14] have studied the influence of workpiece hardness and cutting speed on the chip formation and forces in hard turning of hardened steel AISI H13; whereas, surface integrity was not investigated in this paper. Besides, Chen et al. [15] have investigated the surface micro-topography in hard turning of GCr15 bearing steel by using the polycrystalline cubic boron nitride (PCBN) tools. The results showed that feed rate has greater influence on surface roughness than cutting speed.

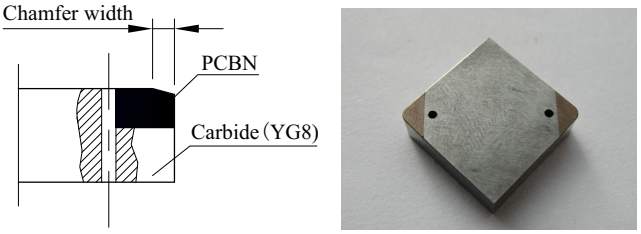

a) Construction of a PCBN insert b) PCBN insert

Fig. 1 Design schematic of composite PCBN insert. **a** Construction of a PCBN insert. **b** PCBN insert

It is well known that the hardened tool steel AISI D2 is a kind of a difficult-to-cut material. However, it is revealed from the literatures reviewed above that, up to present, there are still few studies about focusing on the influence of cutting speed, depth of cut, feed, workpiece hardness, and nose radius on surface integrity in FDHT of the hardened tool steel AISI D2 at different hardness levels in the range from 51 to 65±1 HRC. Here, a study aims to experimentally investigate the effect of these variables on surface integrity and their changing mechanisms. It is of great significance and reference value in understanding the mechanism when FDHT of the hardened tool steel in various hardness levels and further developing the theory of foundations of dry hard cutting and accelerating its application in the production.

2 Experimental procedures

2.1 Workpiece material

In this study, the bar of tool steel AISI D2 (Cr12MoV, China) was used. The chemical composition is presented in Table 1. The bars of 48-mm diameter and 300-mm length were used.

2.2 Heat treatment

In order to effectively utilize the FDHT process in the manufacturing industries, the hardened tool steel at different hardness levels were considered for this study with a polycrystalline cubic boron nitride (PCBN) insert. The results showed that the tool steel AISI D2 could get fine-needle martensite, high diffusion, and uniform distribution fine-grain carbide if using the quenching temperatures of 1000–1040 °C [16]. According to the methods of heat treatment in

Table 1 Chemical composition of the tool steel AISI D2 (wt%)

C	Cr	Mo	Mn	Si	P	S	V
1.55	11.25	0.45	0. 35	0.35	0.025	0.025	0.20

Table 2 The effective geometry parameters of PCBN cutting tools

κ_r/°	κ_r'/°	α/°	γ_0/°	γ_0'/°	λ_s/°	r_ε/mm	β/°	b/mm
65°	25°	−5°	5°	5°	−3°	0.8, 1.2, 1.6	−15°	0.10

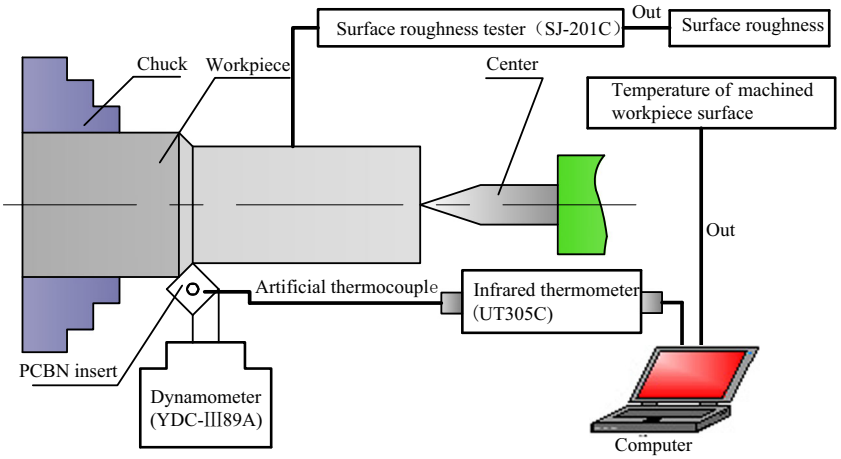

Fig. 2 Schematic diagram of the measurement system

the literature [17], the specimens were inserted into an electrical resistance furnace at 1000–1040 °C, then quenched in oil, and finally tempered at various low temperatures (100, 220, 350, 520, and 550 °C). The hardness values of the differently treated specimens were estimated by Rockwell hardness tester. At least three readings have been taken to estimate the average value of hardness of every specimen. The obtained hardened specimens were in five hardness levels of 51, 55, 58, 62, and 65±1 HRC.

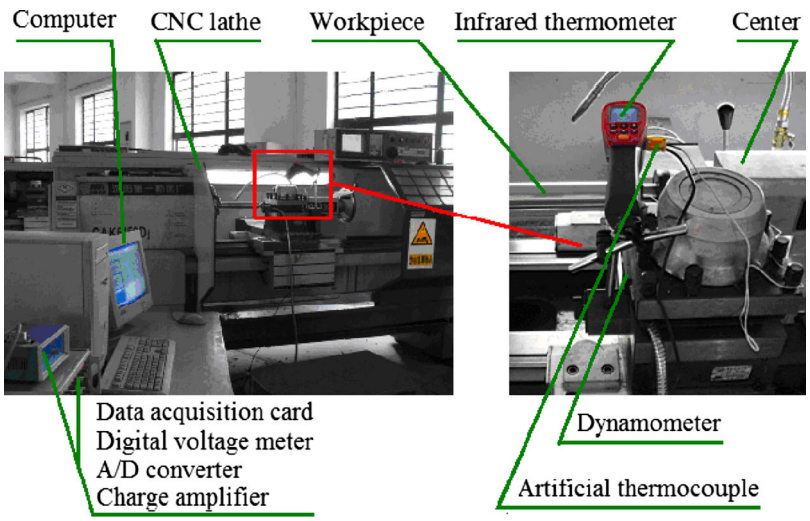

(a) CNC lathe (b) Artificial thermocouple, infrared thermometer, and dynamometer

(c) Surface roughness tester

Fig. 3 Experimental setups. **a** CNC lathe. **b** Artificial thermocouple, infrared thermometer, and dynamometer. **c** Surface roughness tester

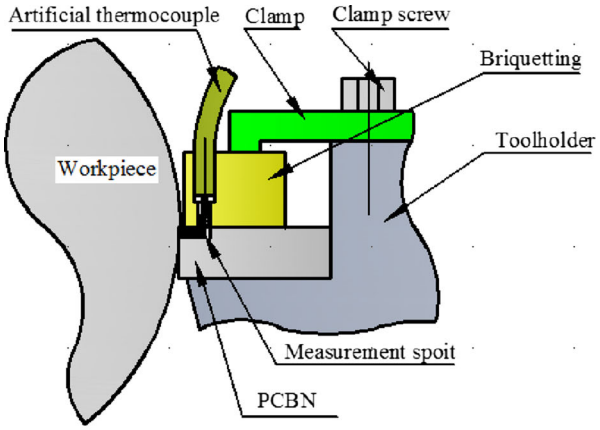

(a) Schematic diagram of the cutting tool temperature measurement

(b) Testing ground of the temperature measurement

Fig. 4 Temperature measurements. **a** Schematic diagram of the cutting tool temperature. **b** Testing ground of the temperature measurement

2.3 PCBN cutting tool

2.3.1 Choice of the contents of CBN

At present, in the tool and die industries, the PCBN tool has been extensively utilized to dry hard machine hardened steel, refractory steel, and high-temperature alloy steel, especially for difficult-to-cut materials with different hardness levels of 55–65±1 HRC [18].

In this paper, according to the literature [19], the PCBN cutting tools (type: GE2100, America) which has an approximate chemical composition of 50 % CBN by volume and a CBN grain size of 2 μm were selected to turn the hardened tool steel at different hardness levels (51–65±1 HRC). In hard cutting, the carbide can provide shock resistance; the CBN provides very high wear resistance and cutting-edge strength. Therefore, the composite PCBN inserts (type: SCGN150404) made in Beijing World Company were utilized to finish dry hard turn hardened workpiece, as shown in Fig. 1.

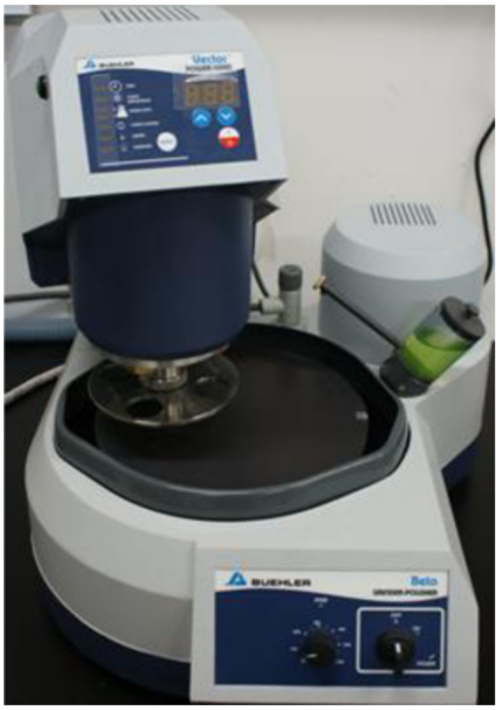

Fig. 5 Semi-automatic Grinding and polishing machine

2.3.2 Geometry parameter of PCBN tool

The inserts were clamped in a piezoelectric three-component turning dynamometer (type: YDC- III89A) tool holder. Except for the nose radius, all the composite PCBN inserts used for the experiments has the same tool geometry parameters. The effective geometry parameters of PCBN cutting tools are presented in Table 2.

2.4 Experimental measurement system and procedures

The measurement system of the experimental investigation was made up of the CNC lathe, dynamometer (type: YDC-III89), infrared thermometer with accessory artificial thermocouple (type: UT305C), scanning electron microscopy (SEM, type: JSM-6700F), and 3D profilemeter (type: Newview5022, America).

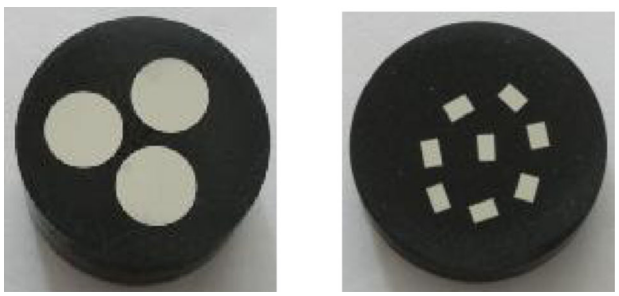

(a) Metallurgical structure (b) White layer

Fig. 6 Finished specimens. **a** Metallurgical structure. **b** White layer

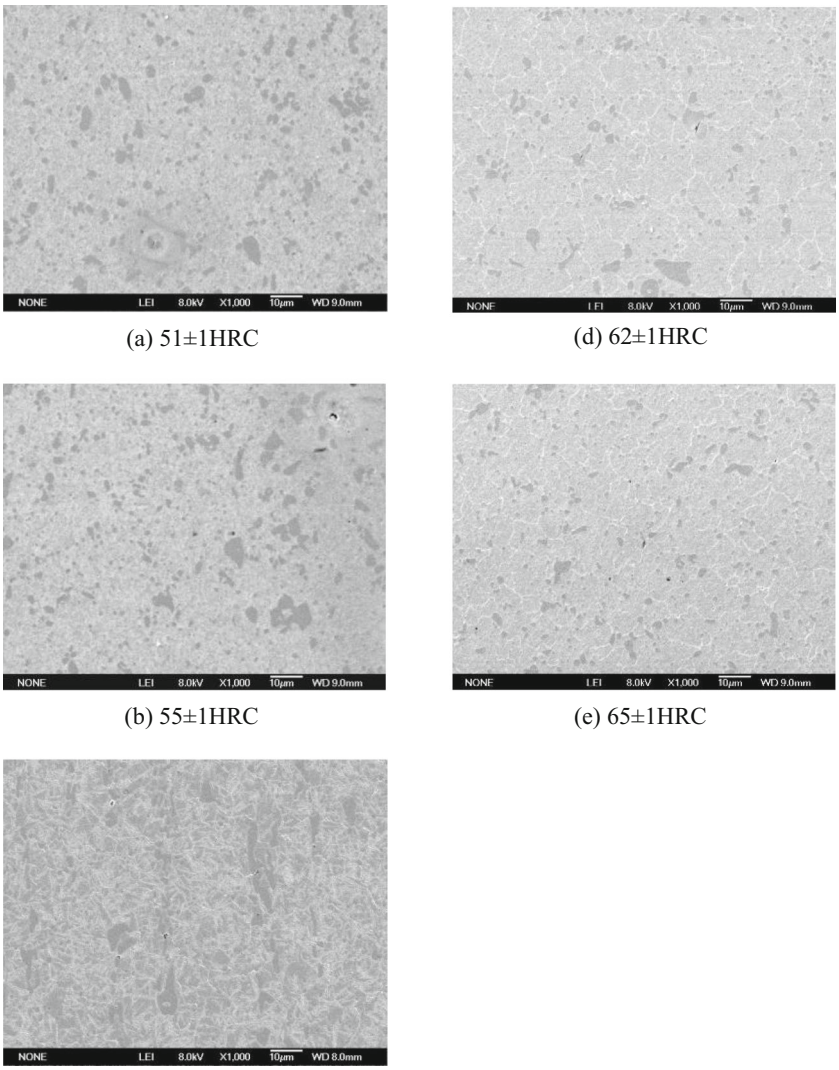

(a) 51±1HRC (d) 62±1HRC

(b) 55±1HRC (e) 65±1HRC

(c) 58±1HRC

Fig. 7 Metallurgical structure of the estimated materials. **a** 51±1 HRC. **b** 55±1 HRC. c 58±1 HRC. d 62±1 HRC. **e** 65±1 HRC

2.4.1 CNC lathe and surface roughness measurements

As presented in Fig. 2, FDHT tests were conducted by using a CNC lathe (Fig. 3a) varying from 0 to 2200 rpm and a maximum power of 9.5 kW at a room temperature of about 22 °C and relative humidity of about 40 %. A portable surface roughness tester made in Japanese (type: SJ-201C, Fig. 3c) was used to measure surface roughness (Ra). Surface roughness was measured seven times in different places along the feed direction after each turning operation.

2.4.2 Temperature measurements

Temperatures of machined workpiece surface were measured by means of an infrared thermometer, and then data was saved in a computer. Temperatures of the cutting tools were measured by using an artificial thermocouple plugged into a small hole of 1.2-mm diameter where it is 2.5 mm distant from the tip of the cutting tool. And temperature of tool was presented on the display of the infrared thermometer when the FDHT was over. Schematic diagram and testing ground of the temperature measurement are described in Fig. 4a, b.

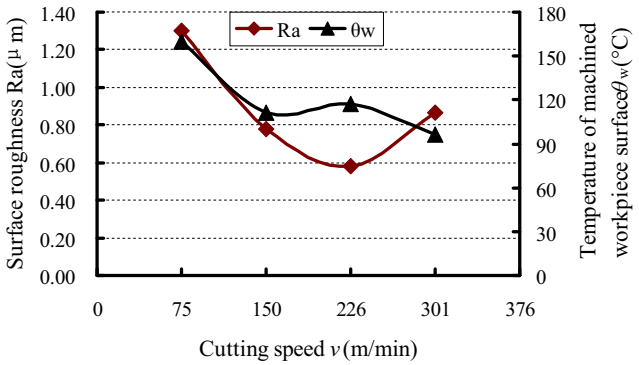

Fig. 8 The effect of the cutting speed on the surface roughness (VB= 0.10–0.15 mm, r_ε=0.4 mm, f=0.10 mm/r, a_p=0.15 mm, H=62±1 HRC)

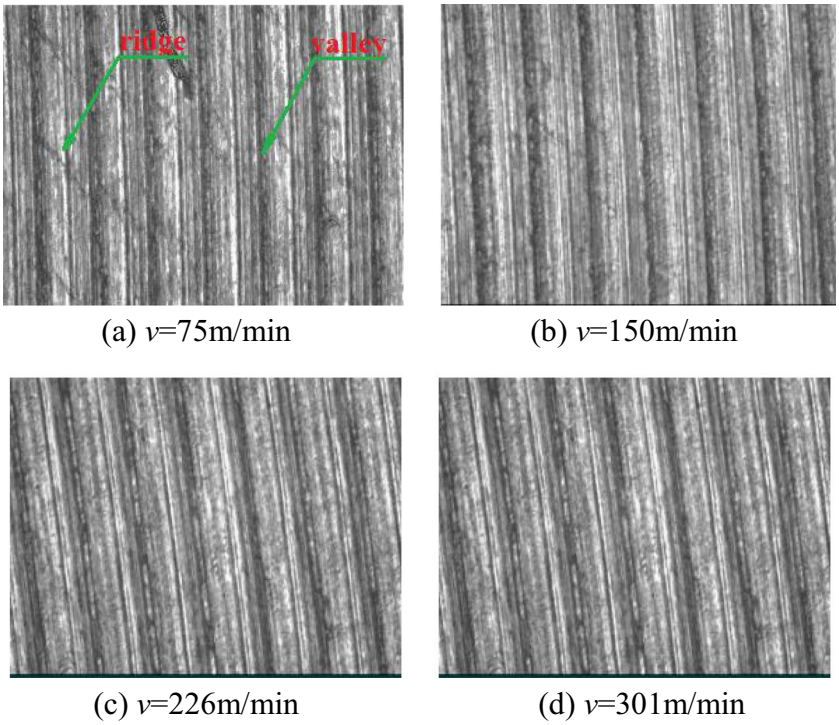

(a) v=75m/min (b) v=150m/min

(c) v=226m/min (d) v=301m/min

Fig. 9 Machined surface morphology (VB=0.10–0.15 mm, r_ε=0.4 mm, f=0.10 mm/r, a_p=0.15 mm, H=62±1 HRC). **a** v=75m/min. **b** v=150m/min. c v=226m/min. **d** v=301m/min

2.4.3 Metallurgical structure and white layer

After mounting, grinding, polishing, and etching (etchant used: 4 % nitric acid alcohol solution for 40 s), microstructural examination of the machined surface were carried out by using a SEM. The polishing has been carried out by using a semiautomatic grinding and polishing machine from Buehler shown in Fig. 5. The processes are as follows:

1. Grinding: using UltraPrep (9 μm) metal-bonded disc at the normal load of 20 N and 120 r/min (rotating direction is the same) for 5 min.
2. Polishing: using surface of preparation with the TriDent polishing cloth (3 μm) of and the MetaDi polishing liquid at the normal load of 25 N and 120 r/min (rotating direction is the same) is for 10 min. Figure 6a, b is the finished specimens.

2.4.4 Morphology of the machined surface

The machined surface morphology examination was carried out by using SEM. The metallographic samples were extracted from the machined surfaces and then analyzed by using a 3D profilemeter. Elemental mapping of the machined surfaces was conducted in a SEM equipped with energy dispersive X-ray spectroscopy (EDS) detector.

3 Results and discussion

3.1 Metallurgical structure

Figure 7a–e presents the SEM micrographs of the metallurgical structure of the hardened tool steel AISI D2 at different

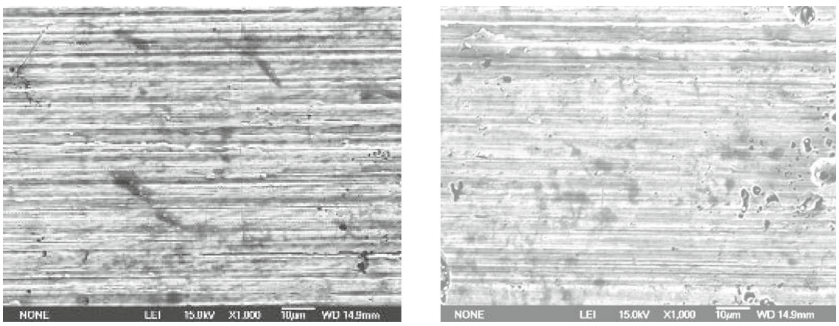

(a) v=75m/min (b) v=301m/min

Fig. 10 Machined surface micrographs (×1000) (VB=0.10–0.15 mm, r_ε=0.4 mm, f=0.10 mm/r, a_p=0.15 mm, H=62±1 HRC). **a** v=75m/min. **b** v=301m/min

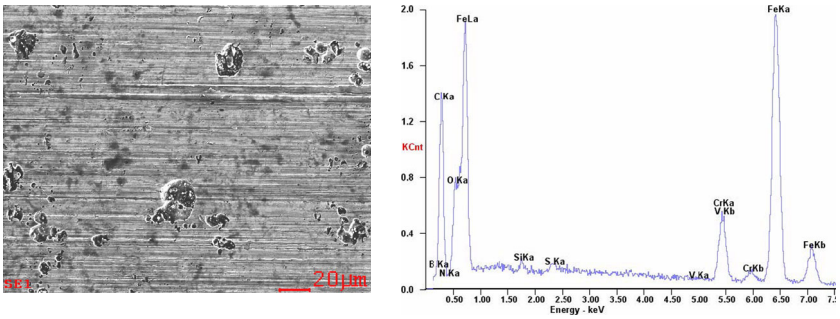

(a) Zone of the element analysis (b) EDS analysis

Fig. 11 Machined surface morphology (VB=0.10–0.15 mm, r_ε=0.4 mm, f=0.10 mm/r, a_p=0.15 mm, H=62±1 HRC). **a** Zone of the element analysis. **b** EDS analysis

hardness levels of 51±1, 55±1, 62±1, 58±1, and 65±1 HRC, respectively. It can be seen from this figure, the lower the hardness the more is the retained austenite. And the metallurgical structures are mainly comprised of the tempered martensite+carbide+retained austenite when the hardness reaches the value as high as 62±1 HRC.

3.2 Effect of cutting speed

Figure 8 shows that the cutting speed has a more important influence on the surface roughness in FDHT of hardened steel AISI D2, especially at lower cutting speeds of 75–226 m/min.

It can be seen from Fig. 8 that the surface roughness firstly decreases and then increases with increments of the cutting speed. As shown clearly in this figure, the surface roughness attains the highest peak of 1.29 μm at a cutting speed of 75 m/min. It also can be observed that the changing law of surface roughness is similar to that of temperature within the machined surface. Therefore, there is a certain relationship between the surface roughness and temperature within the machined surface. These phenomena should be induced by the following further reasons. On the one hand, there are much more serious squeezing and elastic deformation in the tool-workpiece junction zone at slower cutting speeds relative to higher cutting speeds shown in Fig. 10a, b, which induces higher surface roughness values at lower cutting speeds than at higher cutting speeds. However, the surface roughness slightly increases owing to the vibration of cutting tool when the cutting speed exceeds a certain value, which is similar to the literature [20]. On the other hand, built-up edge can cohere with the cutting edge as the cutting temperature attains a certain value which built-up edge disappears. Deformation of built-up edge undergoes such the process as form, increase, and disappearance at this temperature, which induces the cutter marks with different sizes to grow in machined workpiece surface, and hence deteriorates the machined surface finish, as shown in Fig. 9.

It can be clearly observed in Fig. 9 that there are several even and interval feed marks in the machined surface. And the cutter marks at the cutting speed of 150 m/min are clearer compared with other three cutting speeds.

As presented in Fig. 10, the ploughing effect at the cutting speed of 75 m/min is clearer relative to 301 m/min; while the material side flows do not occur. The reasons are as follows: The heat dispersed by chip is much less than that absorbed sufficiently by the machined workpiece surface at a cutting speed of 75 m/min, which is good agreement with the literature [14]. It intenerates metal within the machined surface and then the feature of the tool flank is duplicated on the machined surface, as shown in Fig. 10a. Furthermore, it is interesting that some mysterious materials are presented in the machined surface, as clearly shown in Fig. 10b. The EDS analysis shows these mysterious materials are the oxidation mixture containing the approximate chemical composition of 18.53 % B, 31.41 % C, and 5.04 % O, and so on, as shown in Fig. 11. The reasons

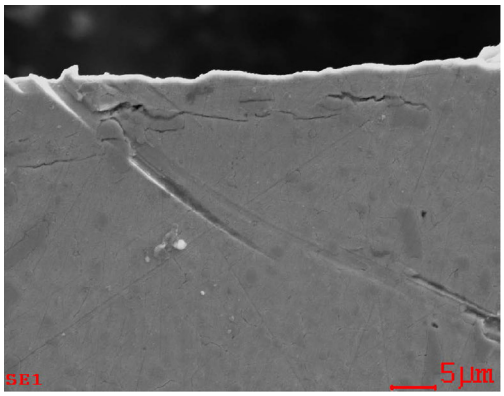

(a) SEM images of white layer

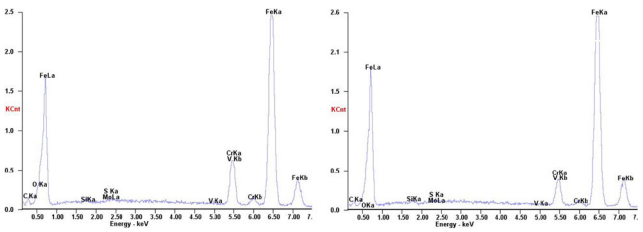

(b) EDS analysis in white layer zone (c) EDS analysis in bulk material zone

Fig. 12 SEM image of subsurface microstructure and EDS analysis. **a** SEM images of white layer. **b** EDS analysis in white layer zone. **c** EDS analysis in bulk material zone

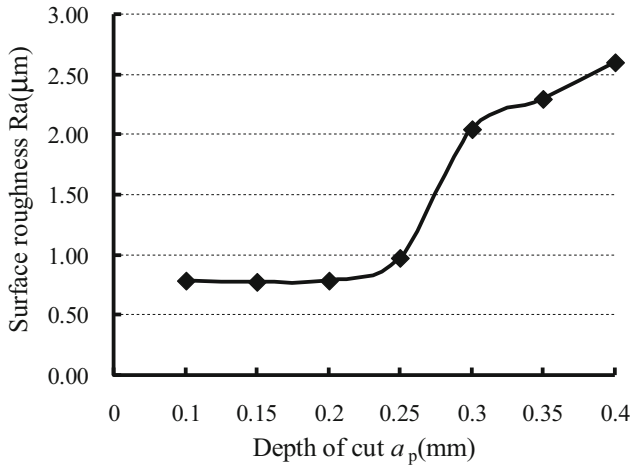

Fig. 13 The effect of depth of cut on the surface roughness (VB=0.10–0.15 mm, v=150 m/min, r_ε=0.4 mm, f=0.10 mm/r, H=62±1 HRC)

are that the FDHT at a 301-m/min cutting speed results in more heat generation and hence some tiny materials in the machined surface are cohered by the cutting tool. These black fusion welding materials later take away the smallest amount of material of the cutting tool and adhere to the newly machined surface, and ultimately cause damage to the machined surface quality, even if the surface roughness is kept within the desired tolerance. This is the reason that the surface roughness at a cutting speed of 301 m/min is higher than that at 226 m/min.

Given all that, the ploughing effect has more significant influence on the surface roughness than those black fusion welding materials, and the surface roughness are in the range of 0.58–0.86 μm when the cutting speed ranges between 150 and 301 m/min and totally attains a surface finish of grinding.

As shown from Fig. 12a that white layer formations can be observed in the case of a 150-m/min cutting speed. Comparing Fig. 12b with Fig. 12c, it can be clearly seen that the carbon content in bulk material zone is higher than that in white layer zone. This may be due to the following reasons. On one hand, instantaneous high temperature and cooling within the machined surface do occur in FDHT, and hence the supersaturated carbon particles separate out in the form of carbide as the austenite converts the martensite. On the other hand, the chemical reaction during turning induces the carburizing effect within the machined surface induced by the chemical reaction during turning can result in carbon diffusing in the white layer zone, and hence this leads to the increase of the carbon content.

3.3 Effect of depth of cut

As shown clearly in Fig. 13, values of the surface roughness do hardly change in the range from 0.10- to 0.25-mm depth of cut, and it is only 0.54 μm at 0.15 mm. This result indicates that the surface roughness is not very sensitive to the depth of cut in the range from 0.10 to 0.25 mm. However, they sharply increase when the depth of cut exceeds 0.25 mm and attain the highest peak of 2.6 μm at a 0.40-mm depth of cut. Figure 16 shows that the surface roughness does deteriorate as the a_p is greater than the h_r. Therefore, the better turning depth of cut should be selected between 0.10 and 0.25 mm and a preferable turning depth of cut is 0.15 mm as turning by using the cutting tool with 0.4-mm nose radius.

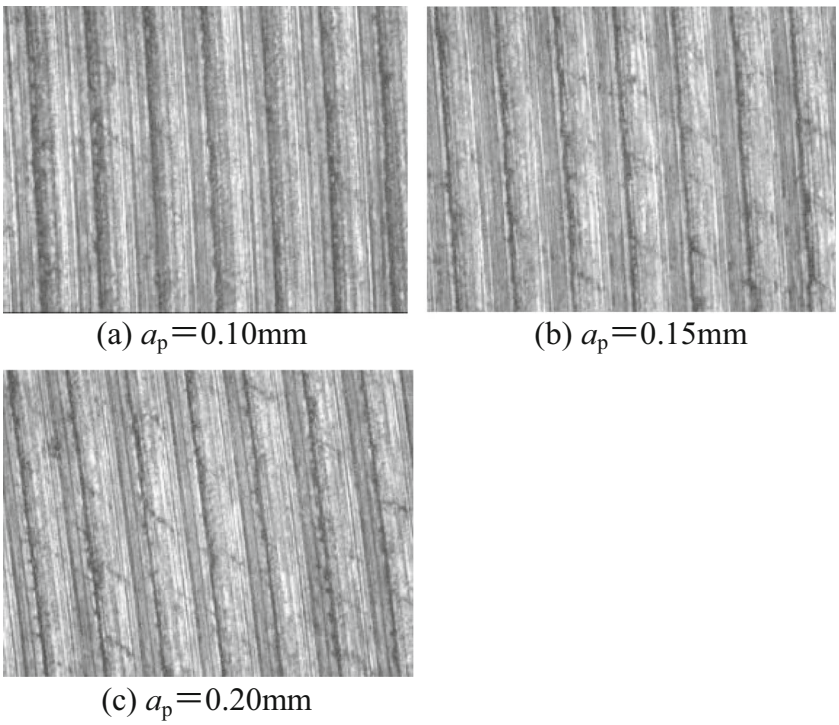

Fig. 14 Machined surface morphology (VB=0.10–0.15 mm, r_ε=0.4 mm, f=0.10 mm/r, v=150 m/min, H=62±1 HRC). **a** ap=0.10 mm. b ap=0.15 mm. **c** ap=0.20 mm

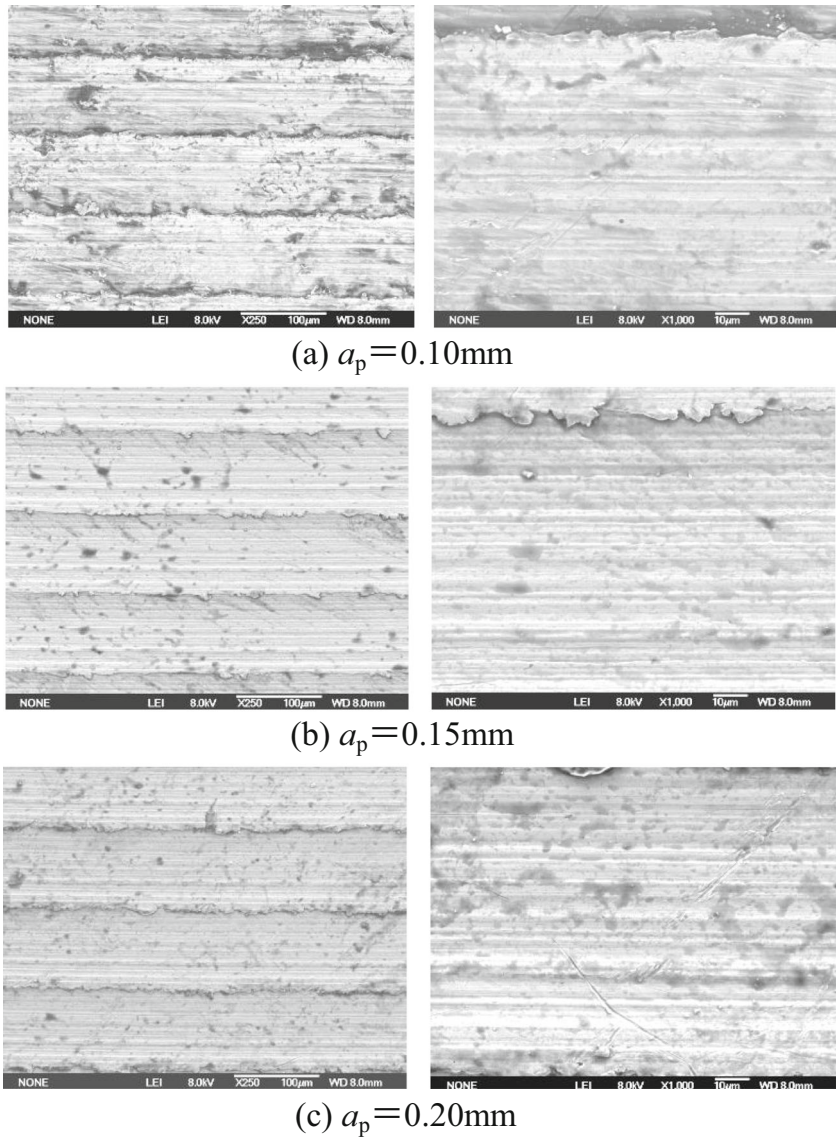

Fig. 15 Machined surface micrographs (×1000) (VB=0.10–0.15 mm, r_ε=0.4 mm, f=0.10 mm/r, v=150 m/min, H=62±1 HRC). **a** ap=0.10 mm. **b** ap=0.15 mm. **c** ap=0.20 mm

Equation (1) shows that only the feed and nose radius have important influence on the surface roughness if only considering the geometric profile; while the influence of the depth of cut is negligible, which has been already verified by the experimental results in this investigation. Moreover, it can

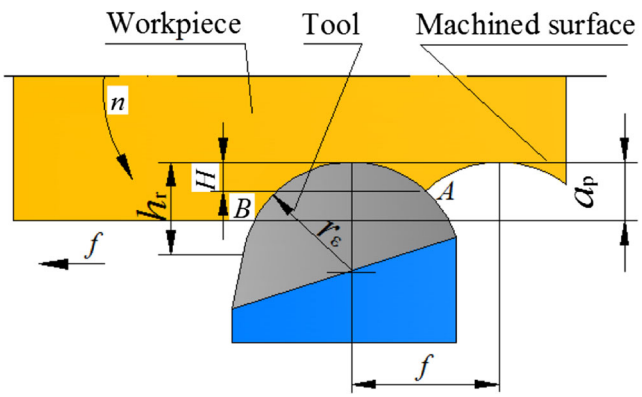

Fig. 16 Geometric mode under the condition of SDOC-LNR-OT

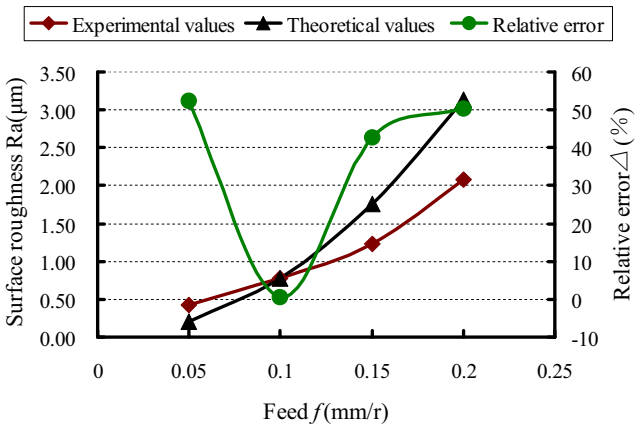

Fig. 17 The effect of feed on the surface roughness (VB=0.10–0.15 mm, v=150 m/min, r_ε=0.4 mm, a_p=0.15 mm, H=62±1 HRC)

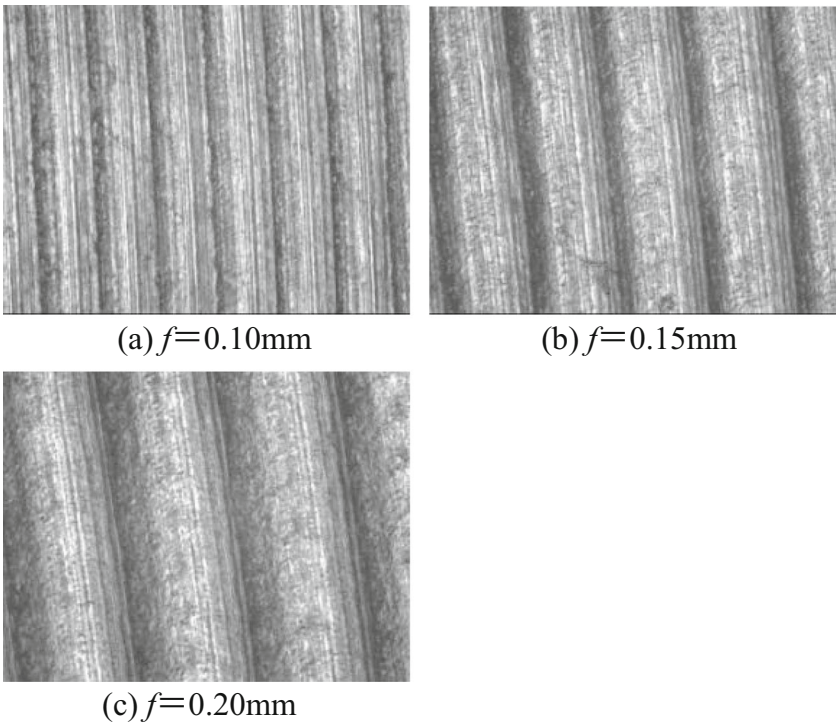

Fig. 18 Machined surface morphology (VB=0.10–0.15 mm, r_ε=0.4 mm, a_p=0.15 mm, v=150 m/min, H=62±1 HRC). **a** f=0.10 mm. b f=0.15 mm. **c** f=0.20 mm

be clearly observed in Fig. 14 that there is but very little influence on the material side flows along the feed marks when the depth of cut increases between 0.10 and 0.20 mm, which also may be one of the possible reasons that the surface roughness keeps mostly unchangeable in the range of 0.10–0.20-mm depth of cut.

Figure 15 represents the effect of depth of cut on the machined surface micrographs by using a SEM. It can be observed in Fig. 15a that the phenomena of "residual cutting" [21] do occur when depth of cuts are less than a certain value (e.g., 0.10 mm). This can be attributed to the following main mechanisms: Firstly, when cutting at smaller depth of cuts using the cutting tool with 0.15-mm flank wear, there is more obvious extrusion effect owing to resilience of workpiece material relative to other larger depth of cuts; secondly, the extrusion effect resulted from the cutting tool flank face acting on "residual cutting" materials increases, while cutting effect decreases, which makes these "residual cutting" materials squeezed by the cutting tool flank face. This result is also verified by the information shown in Fig. 15a.

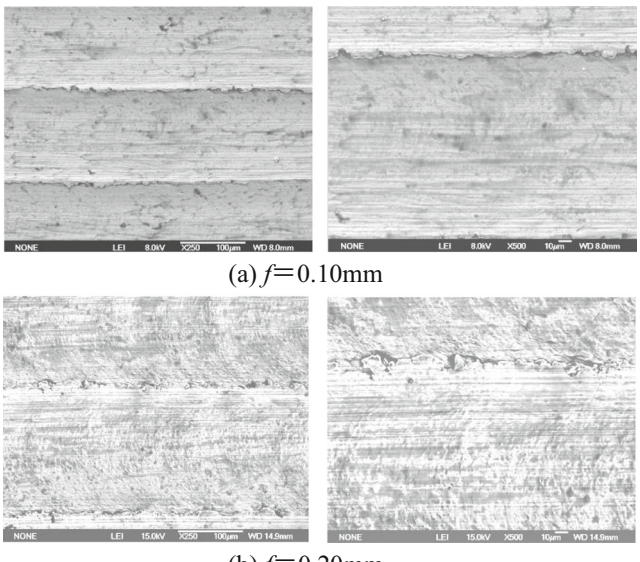

Fig. 19 Machined surface micrographs (VB=0.10–0.15 mm, r_ε=0.4 mm, a_p=0.15 mm, v=150 m/min, H=62±1 HRC). **a** f=0.10 mm. **b** f=0.20 mm

The cutting effect of the cutting tool increases with increments of depth cut, while the squeezing effect of the tool flank face acting on the "residual cutting" materials decreases, as shown explicitly in Fig. 15b, c. Meanwhile, more serious material plastic deformation in the machined surface does occur and even cohesion effect in the machined surface happens because of more heat generation, and then cold welding effect does occur for these cohesion materials due to the sharp decrease of temperature as the cutting tool leaves away. As a result, there are traces of residual materials in the machined surface, which is agreement with the literature [22].

Kishawy and Elbestawi [23] consider that there are two possible mechanisms for material side flow. On the one hand, the material in the tool-workpiece junction zone is subjected to a high enough temperature and squeeze when depth of cut is less than a minimum value (e.g., 0.10 mm). In this investigation, this should be induced by not only the depth of cut but also cutting speed because cutting speed plays a significant

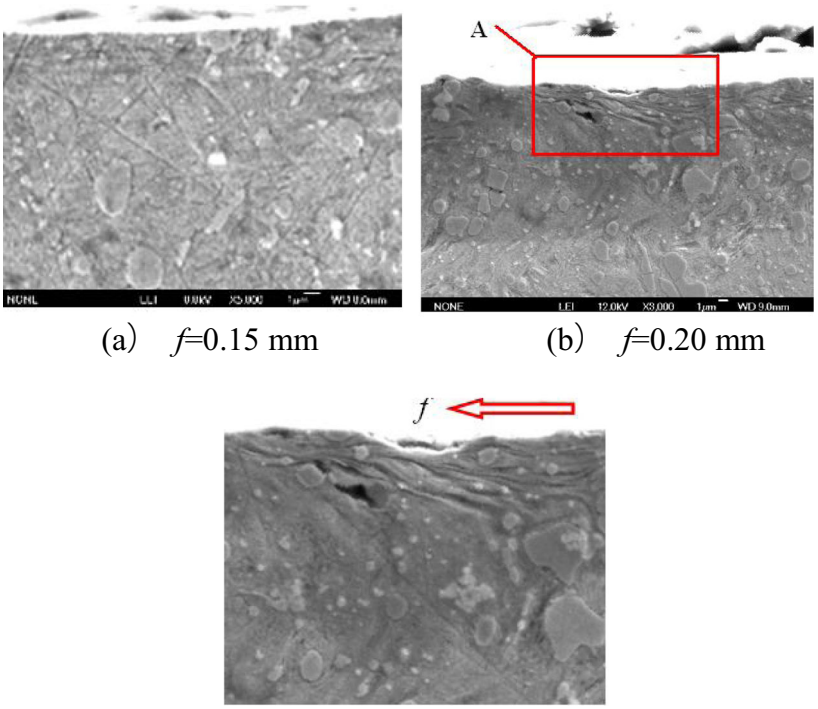

(a) f=0.15 mm (b) f=0.20 mm

(c) SEM images showing severe plastic deformation beneath the machined surface (A zone)

Fig. 20 Machined surface micrographs (VB=0.10–0.15 mm, r_ε=0.4 mm, a_p=0.15 mm, v=150 m/min, H=62±1 HRC). a f=0.15 mm. **b** f=0.20 mm. **c** SEM images showing severe plastic deformation beneath the machined surface (A zone)

role in material soft effect. On the other hand, he considers that the material plasticized in the cutting zone flows through the worn trailing edge to the sides of the tool, which is good agreement with result in this investigation.

3.4 Effect of feed

The profile of surface roughness can be considered as successive movements of the tool at intervals of feeds. Therefore, surface roughness may be influenced by geometrical and physical factors. Figure 16 presents a geometric mode under a condition of smaller depth of cut-larger nose radius-oblique turning (SDOC-LNR-OT). The cutting layer being the same shape with the cutting tool profile is existed in the machined surface when the cutting tool motions along the feed direction, as shown in Fig. 16. It can be seen in this figure that the height H has the important effect on surface roughness. If not considering the effect of the built-up edge, burr, and tool flank wear, the theoretical model for estimating surface roughness as follows [24]:

$$\mathrm{Ra} \approx H = \frac{f^2}{32 r_\varepsilon} \tag{1}$$

where Ra is the average height of surface roughness, f is feed, and r_ε is nose radius of the tool.

Figure 17 represents the effect of the feed on the surface roughness. As expected, surface roughness value is smaller at lower feed and it increases with increments of the feed in the range of 0.05–0.20 mm/r, as shown in Fig. 17. Besides, it also can be observed that the theoretical values calculated by Eq. (1) are higher than experimental values in the range from 0.10 to 0.20-mm/r feed. In order to understand the capability of the theoretical model, the relative errors between the calculated and experimental values are calculated by Eq. (2). As shown evidently in Fig. 17, relative percentage errors increase with increments of the feed. It is interesting that both of them are agreement with each other only in the case of a 0.10-mm/r feed, while there are very large errors as turning at the feeds of

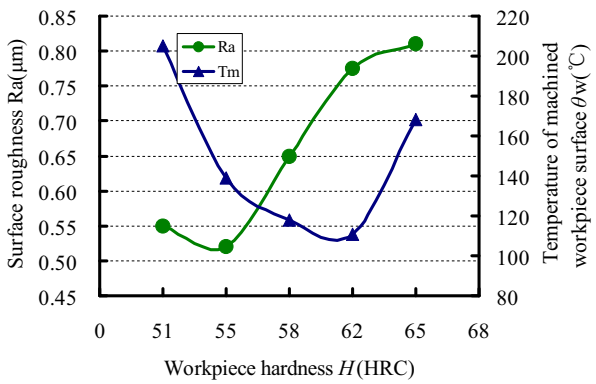

Fig. 21 The effect of workpiece hardness on surface roughness (VB=0.10–0.15 mm, r_ε=0.4 mm, v=150 m/min, a_p=0.15 mm, f=0.10 mm/r)

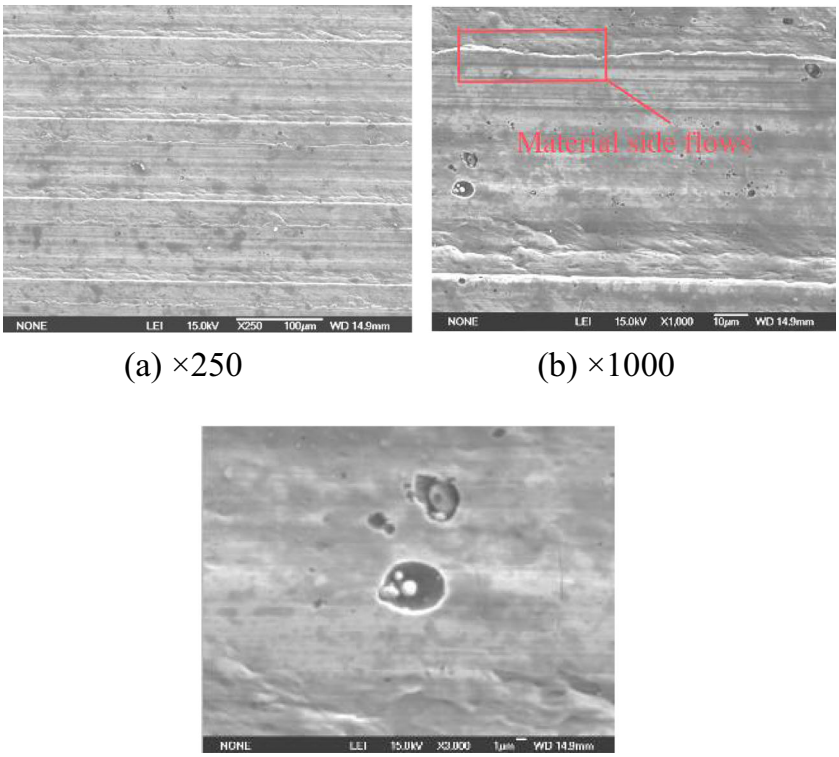

(a) ×250 (b) ×1000

(c) ×3000

Fig. 22 Machined surface micrographs at a hardness of 51± 1 HRC (VB=0.10–0.15 mm, r_ε= 0.4 mm, a_p=0.15 mm, v=150 m/ min). **a** ×250. **b** ×1000. **c** ×3000

0.05, 0.15 and 0.20 mm/r. Therefore, Eq. (1) is limited in application for calculating surface roughness in FDHT of hardened steel.

$$\Delta(\%) = \left|\frac{\mathrm{Ra_{exp}} - \mathrm{Ra_{theo}}}{\mathrm{Ra_{exp}}}\right| \times 100 \quad (2)$$

where $\Delta(\%)$ is the relative error, $\mathrm{Ra_{exp}}$ is the experimental value, and $\mathrm{Ra_{theo}}$ is the theoretical value.

It can be clearly observed in Fig. 18 that the feed has great influence on 3D morphology, and these several even and interval feed marks enlarge with increments of the feed. There are many slight grooves along cutting direction on their sides, as shown in Fig. 18b, c. And these grooves are more obvious on their tops than sides. This may be due to the following two reasons. On one hand, hard inclusions in the cutting tool flank face have the ploughing effect on the machined surface. On the other hand, several slight grooves on the cutting tool flank face resulted from ploughing effect of some hard inclusions in the machined surface do happen, and in turn, they are duplicated; hence, several tiny grooves do occur in the machined surface, as also shown in Fig. 19.

As observed from Fig. 19a that a severe plastic flow arises in the machined surface at lower feed. Although a good

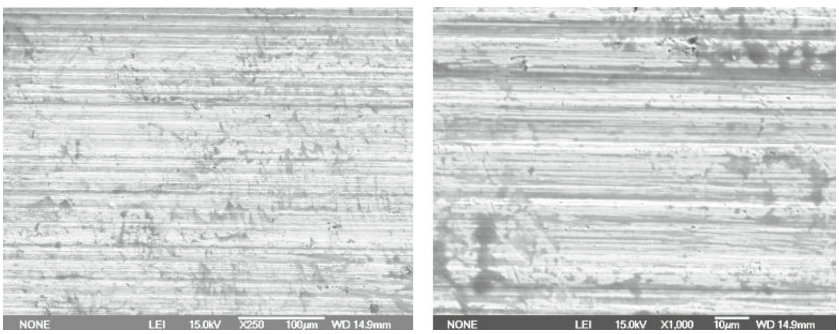

(a) ×250 (b) ×1000

Fig. 23 Machined surface micrographs at a hardness of 58± 1 HRC (VB=0.10–0.15 mm, r_ε= 0.4 mm, a_p=0.15 mm, v=150 m/ min). **a** ×250. **b** ×1000

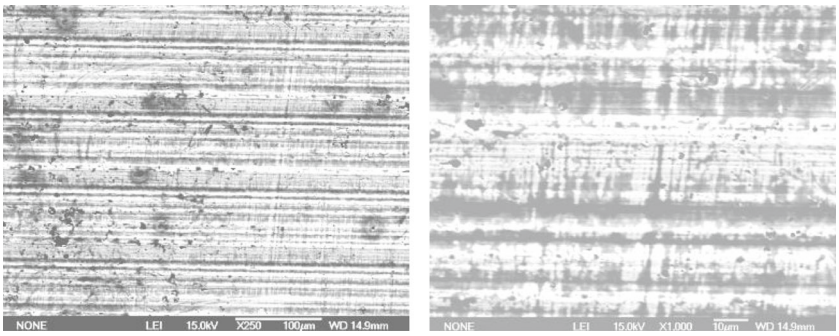

(a) ×250 (b) ×1000

Fig. 24 Machined surface micrographs at a hardness of 62± 1 HRC (VB=0.10–0.15 mm, r_ε= 0.4 mm, a_p=0.15 mm, v=150 m/ min). **a** ×250. **b** ×1000

surface finish is obtained as using the smaller feeds, the experimental results show that extensive material flows also do occur.

Furthermore, it can be shown in Fig. 20 that the subsurface damages produced by the turning process happen, and it becomes severer at the larger feeds. The results indicate that it is the friction on the tool flank face that induces the localized stretch, plastic deformation, and even dilacerations of subsurface material.

3.5 Effect of workpiece hardness

As shown clearly in Fig. 21, a slight drop of surface roughness does occur at a 55-HRC hardness and then they suddenly increase with increments of the workpiece hardness and reach a peak of 0.80 μm at a hardness of 65 HRC. It should be noted that the workpiece hardness has significant affect on the surface roughness in the range from 55- to 62-HRC hardness except in the ranges of 62–65 and 51–55 HRC. Therefore, the cutting difficulty of the hardened workpiece with hardness greater than 50 HRC can be divided into the following different grades: $50<H\leq55$ HRC, easy cutting; $55<H<62$ HRC, moderate cutting; and $H\geq62$ HRC, difficult cutting.

It can be shown in Figs. 22, 23, and 24 that the machined surface material experiences thermal softening and hence the serious material side flows at the feed marks take place and their marks are clearly visible, as shown in Fig. 22. It also can be seen in Fig. 23 that the squeezing effect between the tool flank face and the machined surface make the surface more smooth. Sections of the workpiece were removed from the surface leaving varisized cavities in where several additional recrystallizations can be observed, as shown in Fig. 22c. This phenomenon does occur as heat melting and then condensation, and hence forming crystalline particles. The above results are in agreement with the literature [21].

There is an obvious thermal softening effect in the machined surface at a 58±1-HRC hardness, as shown in Fig. 23. And its machined surface is much smoother compared with that at a 62±1-HRC hardness due to the squeezing effect between the tool flank face and the machined surface; while the feed marks and the ploughing effect at a 62±1-HRC hardness are more significant compared with those at 58±1-HRC hardness, as shown in Fig. 24a. This result seems to be good agreement with Fig. 21. As seen from Fig. 21, the temperatures in the machined surface tend to decrease in the range from 51 to 62-HRC hardness and then do begin to increase at a hardness of 62 HRC, which may be the possible reason that the machined surface at 51 HRC become softer compared with that at 62 HRC.

The element content in the machined surface was analyzed by EDS as FDHT of the hardened AISI D2 steel at a hardness of 58 HRC. It can be observed from Fig. 25, there are a mass of B and N elements transferred from the cutting tool in the tool-workpiece junction zone, which indicates that the transfer of the elements between both of them happened in these tests. Figure 26 presents the changing law of elements in the

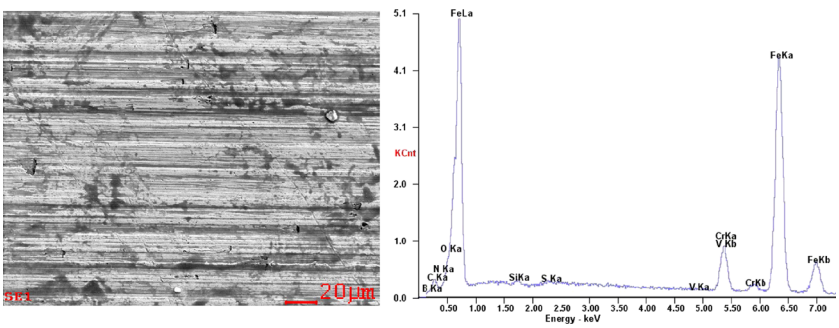

(a) Zone of the element analysis (b) EDS analysis

Fig. 25 Analysis of the elements at a hardness of 58±1 HRC (VB= 0.10–0.15 mm, r_ε=0.4 mm, a_p= 0.15 mm, v=150 m/min). **a** Zone of the element analysis. **b** EDS analysis

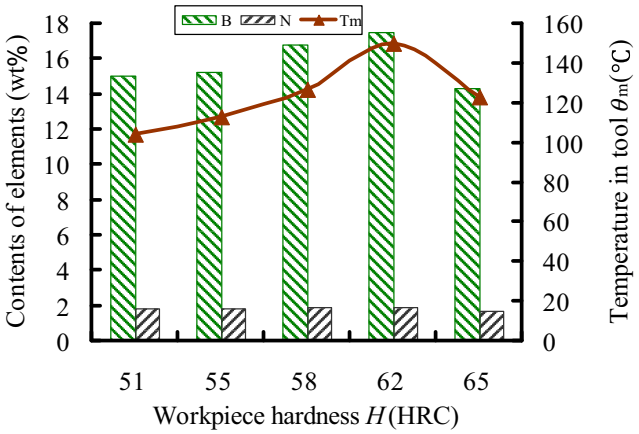

Fig. 26 Variation of B and N elements in the machined workpiece surface and tool temperature (VB=0.10–0.15 mm, r_ε=0.4 mm, a_p= 0.15 mm, v=150 m/min)

machined surface and the cutting tool temperature as turning workpiece with different hardness levels. It is evident that content of B element in the machined surface increases with increments of the workpiece hardness, and then begin to drops at a 62 HRC; while contents of N element largely remain unchanged. It can be observed from this figure that the same trend of B element is mirrored with the cutting tool temperature examined by using an artificial thermocouple; while it is contrary to the temperature in machined workpiece surface, as shown in Fig. 21. These results show that the squeezing effect and temperature of the cutting tool have an important influence on the transferring of the elements in the tool-workpiece junction zone.

3.6 Effect of nose radius

It can be shown from Fig. 27 that values of the surface roughness sharply decrease in the range from 0.4- to 0.8-mm nose radius and attain a lowest value of 0.34 μm at a nose radius of 0.8 mm, which exactly expected from Eq. (1) as the nose radius are 0.4 and 0.8 mm; while they slowly increase in the range from 0.8 to 1.6 mm, which seems to be in contradiction with the experimental results. It shows that the nose radius of the cutting tool have a limited influence on surface roughness at the turning condition given in Fig. 27, compare to the cutting speed, depth of cut, and feed. In fact, there exist following further reasons.

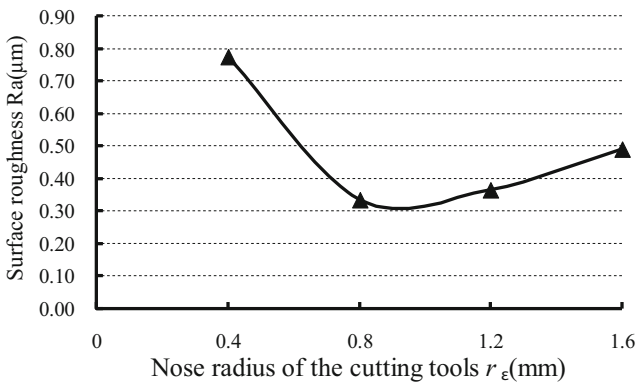

Fig. 27 The effect of nose radius on the surface roughness (VB=0.10–0.15 mm, v=150 m/min, f=0.10 mm/r, a_p=0.15 mm, H=62±1 HRC)

As can be observed from Fig. 16 that the nose radius is far larger compared to the depth of cut and thus cutting takes place only on the nose radius. In this case, the contact length between the cutting edge and the newly machined workpiece surface ($l_r = AB$) can be calculated as follows:

$$l_{\mathrm{r}} = r_\varepsilon \left[\arcsin \frac{\sqrt{a_p\left(2r_\varepsilon - a_p\right)}}{r_\varepsilon} + \arcsin \frac{f}{2r_\varepsilon} \right] .\left(a_p < h_r\right) \quad (3)$$

where h_{r} is a maximum allowable value of depth of cut.

The contact length between the cutting edge and the machined workpiece surface (l_{r}) gradually increases with increments of the nose radius, as shown in Eq. (3). Thus, the heat absorbed by workpiece surface also increases with increments of the contact length l_{r}, and hence, plastic deformation of the machined surface does occur, which may be harmful to the surface roughness. Therefore, the heat effect is greater than the geometry effect as the nose radius attains a certain value (e.g., 0.8 mm in this case).

4 Conclusions

In this paper, experimentations by utilizing FDHT of the hardened tool steel AISI D2 at different hardness levels were conducted with the PCBN tool inserts. The influences of the cutting speed, feed, depth of cut, workpiece hardness, and nose radius on surface roughness in a FDHT process have been analyzed by mean of utilizing various experimental ways and analysis methods. From the previous results, the following conclusions can be drawn:

1. The ploughing, serious squeeze, and elastic deformation effect have more significant effect on the surface roughness than those black fusion welding materials and side flows effect, and the surface roughness are in the range of 0.34–0.86 μm as the cutting speed ranges between 150 and 301 m/min and totally can attain a surface finish of grinding.
2. The surface roughness is not very sensitive to the depth of cut in the range from 0.10 to 0.25 mm. The “residual cutting” materials, more serious material plastic deformation, and even cohesion in the machined surface and cold

welding effect do occur and have influence on the surface integrity.

3. The tiny grooves and severe plastic flow occur in the machined surface, and extensive material flows at lower feeds have important influence on the surface integrity. The subsurface damages produced by the turning process also do occur and become severer at the larger feeds. It is the friction on the tool flank face that induces the localized stretch, plastic deformation, and even dilacerations of subsurface material.
4. The cutting difficulty of the hardened workpiece with hardness greater than 50 HRC can be divided into the following different grades: $50<H\leq55$ HRC, easy cutting; $55<H<62$ HRC, moderate cutting; and $H\geq62$ HRC, difficult cutting. The thermal softening, serious material side flows at the feed marks, squeezing effect between the tool flank face, and the machined surface have significant effect on the surface integrity. Some varisized cavities in the machined surface contains several additional crystalline particles resulted from heat melting and condensation.
5. Values of the surface roughness attain a lowest value of 0.34 μm at a nose radius of 0.8 mm in the range from 0.4 to 1.6-mm nose radius. The heat effect is greater than the geometry effect as the nose radius attains a certain value.

Acknowledgments This investigation was supported by the National Natural Science Foundation of China (Grant No. 51465028) and the Scientific Research Project of Higher Education of Gansu Province (Grant No. 2013A-131 and 2014A-122). The authors wish to thank the anonymous reviewers for their careful review and insightful comments that helped the authors improve this paper.

References

1. Meyer R, Köhler J, Denkena B (2012) Influence of the tool corner radius on the tool wear and process forces during hard turning. Int J Adv Manuf Technol 58(9–12):933–940
2. Yong H, Liang SY (2004) Modeling of CBN tool flank wear progression in finish hard turning. ASME J Manuf Sci Eng 126:98–106
3. Klocke F, Brinksmeier E, Weinert K (2005) Capability profile of hard cutting and grinding processes. Ann CIRP 54(2):552–580
4. Tang L, Huang J, Xie L (2011) Finite element modeling and simulation in dry hard orthogonal cutting AISI D2 tool steel with CBN cutting tool. Int J Adv Manuf Technol 53(9/12):1167–1181
5. Tang L, Gao C, Huang J, Lin X, Zhang J (2013) Experimental investigation of the three-component forces in finish dry hard turning of hardened tool steel at different hardness levels. Int J Adv Manuf Technol 70(9–12):1721–1729
6. Meye R, Köhler J, Denkena B (2011) Influence of the tool corner radius on the tool wear and process forces during hard turning. Int J Adv Manuf Technol 58(2012):933–940
7. Gaitonde VN, Karnik SR, Figueira L, Figueira L, Paulo Davim J (2011) Performance comparison of conventional and wiper ceramic inserts in hard turning through artificial neural network modeling. Int J Adv Manuf Technol 52:101–114
8. Thiele JD, Melkote SN (1999) Effect of cutting edge geometry and workpiece hardness on surface generation in the finish hard turning of AISI 52100 steel. J Mater Process Technol 94:216–226
9. Rech J, Moisan A (2003) Surface integrity in finish hard turning of case-hardened steels. Int J Mach Tool Manuf 43:543–550
10. Ozel T, Hsu TK, Zeren E (2005) Effects of cutting edge geometry, workpiece hardness, feed rate and cutting speed on surface roughness and forces in finish turning of hardened AISI H13 steel. Int J Adv Manuf Technol 25:262–926
11. Umbrello D, Jawahir I (2009) Numerical modeling of the influence of process parameters and work- piece hardness on white layer formation in AISI 52100 steel. Int J Adv Manuf Technol 44:955–968
12. Okada M, Hosokawa A, Tanaka R, Ueda T (2011) Cutting performance of PVD-coated carbide and CBN tools in hardmilling. Int J Mach Tool Manuf 51:127–132
13. Rech J, Moisan A (2013) Surface integrity in finish hard turning of case-hardened steels. Int J Adv Manuf Technol 43:543–550
14. Aouici H, Yallese MA, Chaoui C, Mabrouki T, Rigal JF (2012) Analysis of surface roughness and cutting force components in hard turning with CBN tool: Prediction model and cutting conditions optimization. Measurement 45:344–353
15. Chen T, Li SY, Han BX, Liu GJ (2014) Study on cutting force and surface micro-topography of hard turning of GCr15 steel. Int J Adv Manuf Technol 9–12:1639–1645
16. Zhou AQ, Deng FY (2001) Experimental study on the heat treatment process for Cr12MoV steel. Die Mould Ind 000:55–57
17. Wang LJ, Miao B, Meng XX (2005) Analysis on the hardness and metallographic structure of Cr12MoV Steel under different heat treatment. Die Mould Ind 000:2–56
18. Dogra M, Sharma VS, Sachdeva A, Suri NM, Dureja JS (2010) Tool wear, chip formation and workpiece surface issues in CBN hard turning: a review. Int J Precis Eng Manuf 11(2):341–358
19. Liu Z, Zhou J, Wan Y (2006) Tool materials for high speed machining and their fabrication technologies. Mater Mech Eng 30(5):1–4
20. Pang JZ, Wang MJ, Duan CZ (2009) Surface roughness in high-speed side milling of hardened mold steel. J Dalian Univ Technol 49: 216–221
21. Xu J (2009) Study on high speed cutting hardened steel with the coated insert (CN35). South China University of Technology, Dissertation
22. Fernández-Abia AI, Barreiro J, López de Lacalle LN, Martínez S (2011) Effect of very high cutting speeds on shearing, cutting forces and roughness in dry turning of austenitic stainless steels. Int J Adv Manuf Technol 57:61–69
23. Kishawy H, Elbestawi M (1999) Effects of process parameters on material side flow during hard turning. Int J Mach Tool Manuf 39: 1017–1030
24. Al-Ahmari AMA (2007) Predictive machinability models for a selected hard material in turning operations. J Mater Process Technol 190:305–311